

# Renormalization Effects on Quasi-Two-Dimensional Organic Conductor $\alpha$ -(BEDT-TTF) $_2$ I $_3$

Hiroki ISOBE<sup>1</sup> and Naoto NAGAOSA<sup>1,2</sup>

<sup>1</sup> *Department of Applied Physics, University of Tokyo, Tokyo 113-8656, Japan*

<sup>2</sup> *Cross Correlated Materials Research Group (CMRG) and Correlated Electron Research Group (CERG), ASI, RIKEN, Wako, Saitama 351-0198, Japan*

The quasi-two-dimensional organic semiconductor  $\alpha$ -(BEDT-TTF) $_2$ I $_3$  has an anisotropic linear dispersion with the zero energy gap near the Fermi level. Due to the vanishing density of states at the Fermi level, the Coulomb interaction is unscreened in this material. We study theoretically the effect of the long-range Coulomb interaction and the low energy/long-wavelength behavior of  $\alpha$ -(BEDT-TTF) $_2$ I $_3$  using the renormalization group analysis. The nearly logarithmic enhancement of the velocity reshapes the tilted Dirac cones, and changes the low temperature behavior. We also show the theoretical calculation for the site-selective spin susceptibility, which can be measured by an NMR experiment.

KEYWORDS: organic conductor,  $\alpha$ -(BEDT-TTF) $_2$ I $_3$ , tilted Dirac cone, renormalization group

Salts of organic molecule BEDT-TTF show various electronic phases, such as Mott insulator, charge transfer insulator, semimetal, and superconductor.<sup>1</sup> In addition, there are many types of crystal structures.  $\alpha$ -(BEDT-TTF) $_2$ I $_3$  is one of such organic compounds,<sup>2-4</sup> which consists of alternately stacked BEDT-TTF molecule layers and triiodide (I $_3^-$ ) anion layers. BEDT-TTF molecular planes constitute conducting layers, on which quasi-two-dimensional electronic system is formed. The symmetry of the crystal structure of  $\alpha$ -(BEDT-TTF) $_2$ I $_3$  is low with only the spatial inversion. The unit cell contains four BEDT-TTF molecules, three of which are crystallographically inequivalent [Fig. 1 (a)].

The band calculation predicts that  $\alpha$ -(BEDT-TTF) $_2$ I $_3$  has semimetallic Fermi surface at room temperature and ambient pressure.<sup>1</sup> The first order phase transition to charge-ordered insulating phase<sup>5</sup> occurs at about 135 K with drastic changes in susceptibility<sup>6</sup> and resistivity.<sup>7</sup> At higher pressure, this charge-ordered insulating phase will

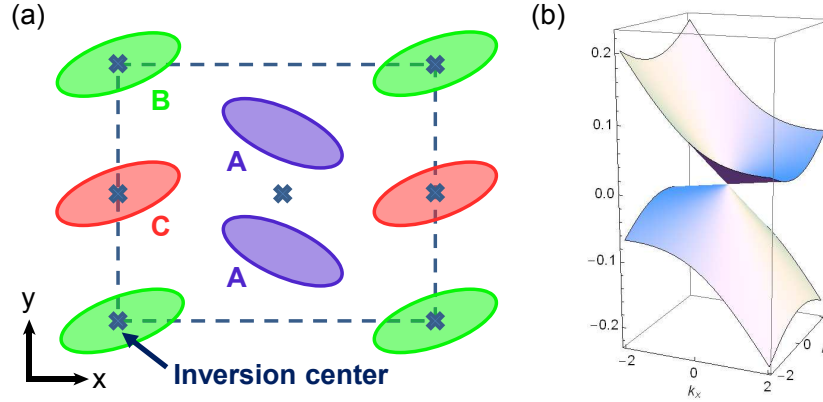


**Fig. 1.** (Color online) (a) The lattice structure of the conducting BEDT-TTF layer. A, B, and C denote the inequivalent sites. The inversion centers are also depicted. (b) The effective energy dispersion near the tilted Dirac cone ( $\xi = +1$ ). The Dirac cone is largely tilted in the  $x$  direction. The units in the graph are  $\text{\AA}^{-1}$  for momentum and eV for energy.

gradually be suppressed, and completely vanishes at 1.5 GPa.<sup>7</sup> It has been revealed that there exists a state with anisotropic linear dispersion near the Fermi level by the band calculation.<sup>8–10</sup> According to this calculation,  $\alpha$ -(BEDT-TTF)<sub>2</sub>I<sub>3</sub> has two strongly tilted Dirac cones, and the tilting is caused by the next-nearest-neighbor hopping. Experimental results, e.g.  $T^2$  dependence of the carrier density,<sup>7,11</sup> are consistent with this linear dispersion.

Graphene<sup>12,13</sup> is a representative material with Dirac cones. Unlike  $\alpha$ -(BEDT-TTF)<sub>2</sub>I<sub>3</sub>, graphene has a purely two dimensional electron system with isotropic Dirac cones. The band crossing point is just on the Fermi level, and vanishing density of states leads to the unscreened long-range Coulomb interaction. It has been analyzed by the renormalization group (RG) approach, and the Dirac cone reshaping due to the renormalized Fermi velocity is observed by Shubnikov-de Haas oscillations as the change in the cyclotron frequency.<sup>14</sup>

Compared to graphene, the narrow band width of  $\alpha$ -(BEDT-TTF)<sub>2</sub>I<sub>3</sub> strengthen the electron correlation effect. It leads to the enhancement of the Dirac cone reshaping, and its effects are expected to be observed more easily compared to graphene. In this paper, we analyze the long-range Coulomb interaction effect on the system with tilted Dirac cones using the RG approach, and calculate the spin susceptibility as a physically measurable quantity.

We start with the following generalized Weyl Hamiltonian describing the tilted mass-

less Dirac cones:<sup>15</sup>

$$\mathcal{H}(\mathbf{k}) = \xi \mathbf{w} \cdot \mathbf{k} + v_x k_x \sigma_x + v_y k_y \sigma_y, \quad (1)$$

where  $\xi = \pm 1$  denotes the valley degeneracy and we put  $\hbar = 1$ . For the moment, we consider the  $\xi = +1$  valley. The parameter  $\mathbf{w}$  determines the tilt of the anisotropic Dirac cone. The energy of this model [Fig. 1 (b)] is

$$E_{\pm}(\mathbf{k}) = \mathbf{w} \cdot \mathbf{k} \pm \sqrt{v_x^2 k_x^2 + v_y^2 k_y^2}. \quad (2)$$

We assume that the parameters satisfy the relation

$$\left(\frac{w_x}{v_x}\right)^2 + \left(\frac{w_y}{v_y}\right)^2 < 1. \quad (3)$$

This condition ensures that the system has a point node.

We consider the anisotropic long-range Coulomb interaction

$$V(\mathbf{q}) = \frac{2\pi e^2}{\varepsilon \sqrt{q_x^2 + \eta q_y^2}} \quad (4)$$

as a perturbation to the system. The anisotropy is reflected in the factor  $\eta$ , and  $\varepsilon$  is the dielectric constant. The unperturbed Green's function is

$$G_0(\mathbf{k}, \omega) = \frac{1}{\omega - \mathbf{w} \cdot \mathbf{k} - v_x k_x \sigma_x - v_y k_y \sigma_y}. \quad (5)$$

The RG analysis for two-dimensional systems often treats Coulomb interaction with large- $N$  expansion.<sup>16,17</sup> In the method for the isotropic system, the Coulomb propagator  $D_0(\mathbf{k}, \omega)$  is modified by adding one-loop fermion bubble diagram with  $N$  fermion species:

$$D_0(\mathbf{k}, \omega) = \left( 2|\mathbf{k}| + \frac{Ne^2}{8\varepsilon} \frac{\mathbf{k}^2}{\sqrt{v^2 \mathbf{k}^2 - \omega^2}} \right)^{-1}. \quad (6)$$

The dressed term has importance in the strong coupling limit, but in the weak coupling case, it gives only small correction to the result. We concentrate our analysis on the low temperature region, where the running coupling constant becomes smaller than the bare value, so the dressed term is neglected in the following analysis.

With the RG analysis, the parameters  $\mathbf{v}$  and  $\mathbf{w}$  are modified by the electron self-energy  $\Sigma(\mathbf{k}, \omega)$ . We calculate the self-energy to one-loop order. The one-loop order self-energy  $\Sigma^{(1)}(\mathbf{k}, \omega)$  [Fig. 2] is evaluated by

$$\Sigma^{(1)}(\mathbf{k}, \omega) = i \int \frac{d\omega'}{2\pi} \frac{d^2 p}{(2\pi)^2} G_0(\mathbf{p}, \omega + \omega') V(\mathbf{k} - \mathbf{p}). \quad (7)$$

The momentum integral is done in the momentum shell  $\Lambda e^{-l} \leq |\mathbf{p}| \leq \Lambda$ . After some

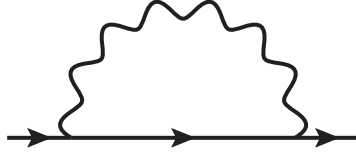


**Fig. 2.** The one-loop self-energy considered for RG analysis.

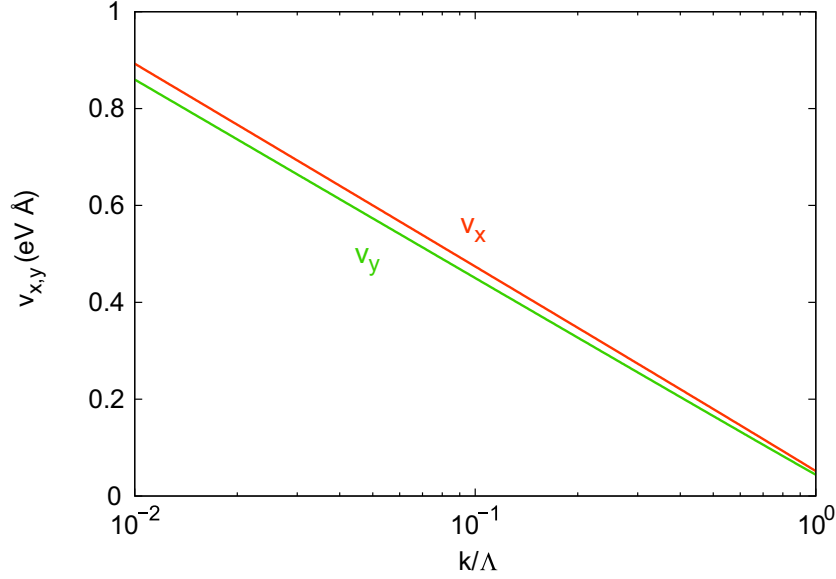


**Fig. 3.** (Color online) The numerical solutions to the RG equations. Both  $v_x$  and  $v_y$  show almost completely logarithmic dependence to the momentum scale.

calculation, we obtain

$$\Sigma^{(1)}(\mathbf{k}, \omega) = \frac{\alpha_x}{4} v_x l k_x \sigma_x + \frac{\alpha_y}{4} v_y l k_y \sigma_y, \quad (8)$$

where the coupling constants  $\alpha_x$  and  $\alpha_y$  are defined by

$$\alpha_x = \frac{2e^2}{\varepsilon\pi} \int_0^{\pi/2} \frac{\cos^2 \theta d\theta}{(v_x^2 \cos^2 \theta + v_y^2 \sin^2 \theta)^{\frac{1}{2}} (\cos^2 \theta + \eta \sin^2 \theta)^{\frac{3}{2}}}, \quad (9a)$$

$$\alpha_y = \frac{2e^2}{\varepsilon\pi} \int_0^{\pi/2} \frac{\sin^2 \theta d\theta}{(v_x^2 \cos^2 \theta + v_y^2 \sin^2 \theta)^{\frac{1}{2}} (\cos^2 \theta + \eta \sin^2 \theta)^{\frac{3}{2}}}. \quad (9b)$$

Then, the RG equations for  $v_x$  and  $v_y$  are

$$\frac{dv_x}{dl} = \frac{\alpha_x}{4} v_x, \quad (10a)$$

$$\frac{dv_y}{dl} = \frac{\alpha_y}{4} v_y. \quad (10b)$$

To one-loop level of the self-energy, the tilting parameter  $\mathbf{w}$  is not renormalized, and

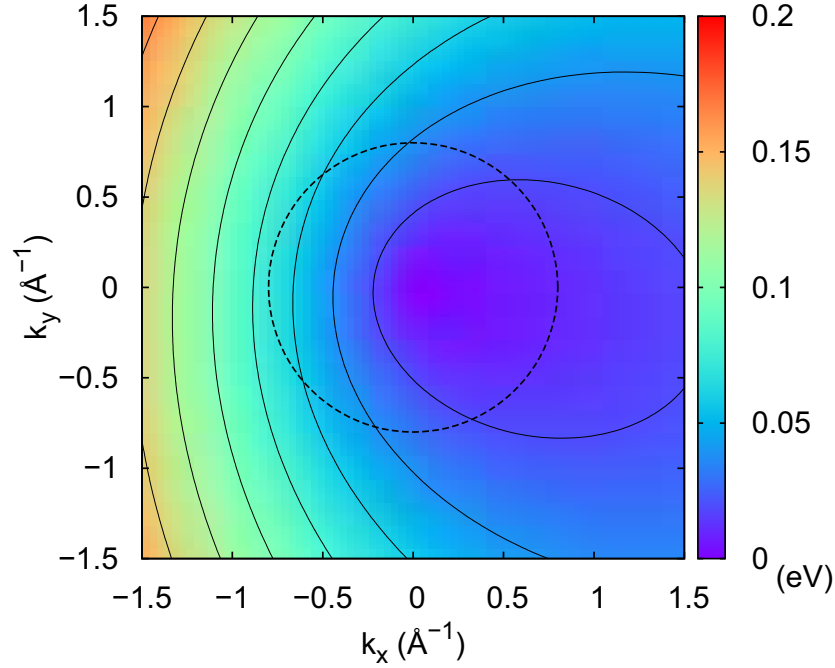


**Fig. 4.** (Color online) The energy distribution in the  $k$ -plane. The cutoff wavelength circle  $\Lambda = 0.8 \text{ \AA}^{-1}$  is shown by the dashed line. The solid lines denote the constant energy curves, plotted every  $0.02 \text{ eV}$ .

stays constant. The discussions above are unchanged for the  $\xi = -1$  valley.

The numerical solutions to Eq. (10) are shown in Fig. 3. The initial values at the cutoff momentum are  $v_x = 0.0515$ ,  $v_y = 0.0439$ ,  $w_x = -0.0389$ ,  $w_y = 0.0048$  (in  $\text{eV \AA}$ ),<sup>18</sup> and we set  $\varepsilon = 10$  and  $\eta = 1$ .  $v_x$  and  $v_y$  show nearly logarithmic dependence on the momentum scale like the system with the isotropic Dirac cone.

The site-selective spin susceptibility  $\chi_\alpha$  ( $\alpha = \text{A, B, and C}$ ) is described by

$$\chi_\alpha = \int_{-\infty}^{\infty} d\epsilon D_\alpha(\epsilon) \left( -\frac{\partial f}{\partial \epsilon} \right), \quad (11)$$

where  $D_\alpha(\epsilon)$  is the site-dependent density of states (DOS), and  $f(\epsilon)$  is the Fermi distribution.<sup>18</sup> The site-dependent DOS has the angular dependence in  $k$ -plane. The DOS of site C mainly comes from the gentle slope of the tilted Dirac cone ( $\theta \sim 0$ ), and the DOS of site B comes from the steep slope ( $\theta \sim \pi$ ). Site A has almost no angular dependence. Thus, the site-dependent DOS for each site shows different angular dependence. Site C, which corresponds to the gentle slope of the tilted Dirac cone, gives the largest contribution to the spin susceptibility, because it has the largest density of states among the three sites. On the contrary, site B brings the smallest spin susceptibility. Although the site-dependent DOS leads to the different magnitude of the site-selective

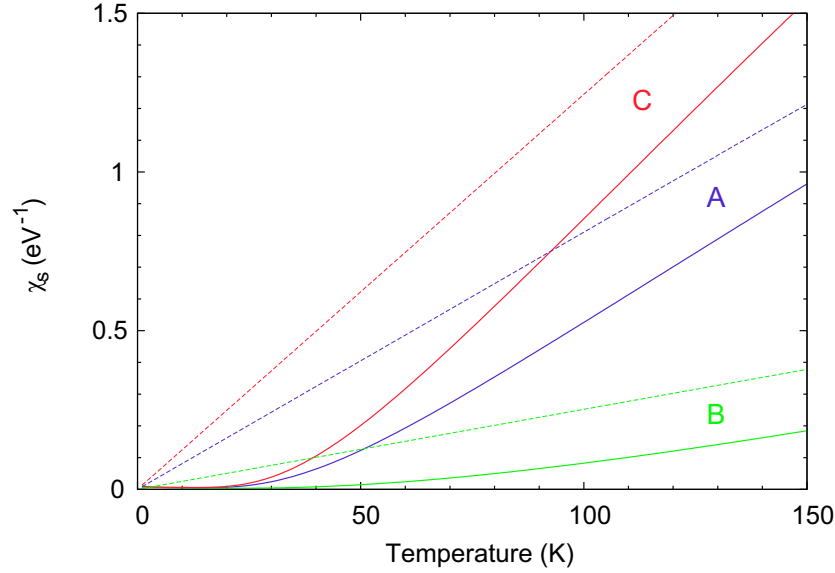


**Fig. 5.** (Color online) The theoretical calculation of the site-selective spin susceptibility. The solid lines and dashed lines describe the spin susceptibility for the interacting and the noninteracting case, respectively.

spin susceptibility, the DOS for each site is proportional to the energy  $\epsilon$ . We can easily see that  $\chi_\alpha \propto T$  in the noninteracting system.

For a two-dimensional system with linear dispersion, the density of states (DOS)  $D(\epsilon)$  is proportional to the energy  $\epsilon$ . However, the enhancement of the velocities by the RG analysis changes the energy dispersion, and sufficiently below the cutoff energy, the density of states as a function of the energy is suppressed compared to the noninteracting one. This scheme is valid for  $\alpha$ -(BEDT-TTF)<sub>2</sub>I<sub>3</sub> within the temperature range where the dispersion is well approximated by a linear one.

The theoretical result for the site-selective spin susceptibility is obtained by numerical calculation, and it is shown in Fig. 5. We set the cutoff wavelength  $\Lambda = 0.8 \text{ \AA}^{-1}$ . Compared to the noninteracting result, which shows linear dependence of  $\chi_\alpha$  in  $T$ , the RG analysis brings the reduction of the spin susceptibility  $\chi_\alpha$  at low temperatures. The validity of the linear dispersion approximation depends also on the angle  $\theta$ . The temperature ranges where the linear dispersion approximation holds are  $T \lesssim 70 \text{ K}$  for the gentle slope and  $T \lesssim 100 \text{ K}$  for the steep slope.

Another important behavior is that the characteristic temperature of the site-selective spin susceptibility  $\chi_\alpha$  is different for each site. Here, the characteristic temperature indicates the point where the spin susceptibility rapidly grows. Although we

set the circular cutoff momentum, the energy at the cutoff depends on the momentum direction due to the tilting of the Dirac cone. This fact leads to the strong suppression of the site-B spin susceptibility.

In summary, we have studied the effect of the long-range Coulomb interaction in the system with tilted Dirac cones using the perturbative RG analysis. The velocity enhances logarithmically as observed in the isotropic case like graphene. We calculate the site-selective spin susceptibility for the quasi-two-dimensional organic conductor  $\alpha$ -(BEDT-TTF)<sub>2</sub>I<sub>3</sub>. The RG analysis reduces the site-selective spin susceptibility at low temperatures, and the characteristic temperatures are different for each site.

We thank M. Hirata and K. Kanoda for useful discussion. This work is supported by Grant-in-Aid for Scientific Research (Grants No. 24244054) from the Ministry of Education, Culture, Sports, Science and Technology of Japan, Strategic International Cooperative Program (Joint Research Type) from Japan Science and Technology Agency, and Funding Program for World-Leading Innovative RD on Science and Technology (FIRST Program).

## References

- 1) H. Seo, C. Hotta, and H. Fukuyama: Chem. Rev. **104** (2004) 5005.
- 2) K. Bender, I. Hennig, D. Schweitzer, K. Dietz, H. Endres, and H.J. Keller: Mol. Cryst. Liq. Cryst. **108** (1984) 359.
- 3) N. Tajima and K. Kajita: Sci. Technol. Adv. Mater. **10** (2009) 024308.
- 4) A. Kobayashi, S. Katayama, and Y. Suzumura: Sci. Technol. Adv. Mater. **10** (2009) 024309.
- 5) H. Kino and H. Fukuyama: J. Phys. Soc. Jpn. **64** (1995) 1877.
- 6) B. Rothaemel, L. Forró, J. R. Cooper, J. S. Schilling, M. Weger, P. Bele, H. Brunner, D. Schweitzer, and H.J. Keller: Phys. Rev. B **34** (1986) 704.
- 7) N. Tajima, S. Sugawara, M. Tamura, Y. Nishio, and K. Kajita: J. Phys. Soc. Jpn. **75** (2006) 051010.
- 8) H. Kino and T. Miyazaki: J. Phys. Soc. Jpn. **75** (2000) 034704.
- 9) S. Katayama, A. Kobayashi, and Y. Suzumura, J. Phys. Soc. Jpn: **75** (2006) 054705.
- 10) A. Kobayashi, S. Katayama, Y. Suzumura, and H. Fukuyama: J. Phys. Soc. Jpn. **76** (2007) 034711.
- 11) K. Kajita, T. Ojio, H. Fujii, Y. Nishio, H. Kobayashi, A. Kobayashi, and R. Kato: J. Phys. Soc. Jpn. **61** (1992) 23.
- 12) K.S. Novoselov, A.K. Geim, S.V. Morozov, D Jiang, M.I. Katsnelson, I.V. Grigorieva, S.V. Dubonos, and A.A. Firsov: Nature **438** (2005) 197.
- 13) Y. Zhang, Y.-W. Tan, H.L. Stormer, and P. Kim: Nature **438** (2005) 201.
- 14) D.C. Elias, R.V. Gorbachev, A.S. Mayorov, S.V. Morozov, A.A. Zhukov, P. Blake, L.A. Ponomarenko, I.V. Grigorieva, K.S. Novoselov, F. Guinea, and A.K. Geim: Nat. Phys. **7** (2011) 701.
- 15) M.O. Goerbig, J.-N. Fuchs, G. Montambaux, and F. Piéchon: Phys. Rev. B **78** (2008) 045415.
- 16) J. González, F. Guinea, and M.A.H. Vozmediano: Phys. Rev. B **59** (1999) R2474.
- 17) D.T. Son: Phys. Rev. B **75** (2007) 235423.
- 18) S. Katayama, A. Kobayashi, and Y. Suzumura: Eur. Phys. J. B **67** (2009) 139.